Surface Heat Budgets and Sea Surface Temperature in the Pacific Warm Pool during TOGA COARE

SHU-HSIEN CHOU

Laboratory for Atmospheres, NASA Goddard Space Flight Center, Greenbelt, Maryland

WENZHONG ZHAO

SM&A Corporation, Largo, Maryland

MING-DAH CHOU

Laboratory for Atmospheres, NASA Goddard Space Flight Center, Greenbelt, Maryland

(Manuscript received 8 October 1998, in final form 10 February 1999)

ABSTRACT

The daily mean heat and momentum fluxes at the surface derived from the Special Sensor Microwave/Imager and Japan's Geostationary Meteorological Satellite radiance measurements are used to study the temporal and spatial variability of the surface energy budgets and their relationship to the sea surface temperature during the Coupled Ocean–Atmosphere Response Experiment intensive observing period (IOP). For three time legs observed during the IOP, the retrieved surface fluxes compare reasonably well with those from the Improved Meteorological Instrument (IMET) buoy, RV *Moana Wave,* and RV *Wecoma.* The characteristics of surface heat and momentum fluxes are very different between the southern and northern warm pool. In the southern warm pool, the net surface heat flux is dominated by solar radiation, which is, in turn, modulated by the two Madden–Julian oscillations. The surface winds are generally weak, leading to a shallow ocean mixed layer. The solar radiation penetrating through the bottom of the mixed layer is significant, and the change in the sea surface temperature during the IOP does not follow the net surface heat flux. In the northern warm pool, the northeasterly trade wind is strong and undergoes strong seasonal variation. The variation of the net surface heat flux is dominated by evaporation. The two westerly wind bursts associated with the Madden–Julian oscillations seem to have little effect on the net surface heat flux. The ocean mixed layer is deep, and the solar radiation penetrating through the bottom of the mixed layer is small. As opposed to the southern warm pool, the trend of the sea surface temperature in the northern warm pool during the IOP is in agreement with the variation of the net heat flux at the surface.

1. Introduction

The western equatorial Pacific is characterized by the highest sea surface temperature (SST) and the heaviest rainfall in the world ocean. A small variation of SST associated with the eastward shift of the warm pool during El Niño–Southern Oscillation events changes the atmospheric circulation pattern and affects the global climate. The change in the SST pattern in the warm pool for a timescale longer than a year is related to the ocean dynamics in the Pacific basin. For a seasonal timescale and shorter, on the other hand, the SST in the warm pool is mainly determined by the surface fluxes and the depth of the ocean mixed layer, which are affected by the variations in the surface wind and clouds.

In a study of the depth of ocean mixed layer with a vertically uniform density in the Pacific warm pool, Lukas and Lindstrom (1991) have found that the mixed layer in this region is very shallow with a mean of ~29 m. The shallow mixed layer reduces the solar heating of the layer because of the enhanced penetration of solar radiation through the bottom of the layer (e.g., Paulson and Simpson 1977; Lewis et al. 1990; Siegel et al. 1995). Between the bottom of the mixed layer and the top of the thermocline, there has been observed to be a barrier layer characterized by nearly constant temperature with stable stratification due to downward increase of salinity (Lukas and Lindstrom 1991; Sprintall and Tomczak 1992; Anderson et al. 1996; Ando and McPhaden 1997). This stable barrier layer inhibits the entrainment of cold water from the deeper thermocline

Corresponding author address: Dr. Shu-Hsien Chou, Code 912, Laboratory for Atmospheres, NASA Goddard Space Flight Center, Greenbelt, MD 20771.
E-mail: chou@agnes.gsfc.nasa.gov

except during very strong westerly wind bursts and is very important to the ocean mixed layer heat budget.

The horizontal advection of heat in the warm pool has been estimated to be generally very small due to a small SST gradient and weak currents (Niiler and Stevenson 1982; Enfield 1986; Godfrey and Lindstrom 1989). Recently, some studies have suggested that the advection of heat may be important to the warm pool heat budget during strong wind events (Cronin and McPhaden 1997; Ralph et al. 1997; Feng et al. 1998; Godfrey et al. 1998). On the other hand, the one-dimensional model of Anderson et al. (1996) has successfully simulated the evolution of the SST in the warm pool during the same period under investigation. For simplicity, we will also neglect the horizontal advection of heat for the investigation of ocean mixed layer heat budget in the warm pool.

In recognition of the importance of the Pacific warm pool in affecting the global climate, extensive measurements were carried out during the intensive observing period (IOP), from November 1992 to February 1993, of the Tropical Ocean Global Atmosphere (TOGA) Coupled Ocean–Atmosphere Response Experiment (COARE) with a major objective of better understanding various physical processes responsible for the SST variation (Webster and Lukas 1992; Godfrey et al. 1998). Various flux measurement programs were carried out at the intensive flux array (IFA) within the region 1°N–5°S and 150°–160°E during the IOP. Radiative, turbulent, and freshwater fluxes at the surface were either directly measured or derived from the measurements of surface temperature, humidity, and winds at the Improved Meteorological Instrument (IMET) buoy (1.75°S, 156°E) and two research vessels (RV), the *Moana Wave* (1.7°S, 156°E) and the *Wecoma* (cruised in a butterfly pattern around the IMET buoy). These high temporal resolution fluxes are very useful for studying the air–sea interaction and for validating the satellite retrievals of surface radiative and turbulent fluxes.

In the western equatorial Pacific, the surface winds are weak and are interrupted intermittently by westerly wind bursts. These westerly wind bursts are often related to the Madden–Julian oscillations (MJOs) that have a period of ~40–50 days (Madden and Julian 1994). During the COARE IOP, there were two MJOs propagating eastward from the Indian Ocean to the central Pacific (Gutzler et al. 1994; Lin and Johnson 1996; Lau and Sui 1997; Sui et al. 1997; Godfrey et al. 1998). Two envelopes of individual cloud clusters and two low-level westerly wind bursts lasting for about 2–3 weeks were associated with the two MJOs. The super cloud clusters reduce solar heating, while the westerly wind bursts enhance the evaporative cooling. Both have an important impact on the SST variation of the warm pool.

A number of techniques have been developed to retrieve air–sea radiative and turbulent fluxes from satellite observations (e.g., Chou et al. 1995, 1997; Chou et al. 1998; Clayson and Curry 1996; Schlussel et al. 1995; Schulz et al. 1997; Zhang et al. 1995; Curry et al. 1999). In a study of the radiation budgets of the Pacific warm pool, Chou et al. (1998) applied empirical relationships between the surface-measured radiative fluxes and the satellite-measured radiances to compute the solar and thermal infrared fluxes over the Pacific warm pool for the COARE IOP. Chou et al. (1997) computed daily mean turbulent fluxes at the surface with a stability-dependent bulk scheme. The surface wind and humidity retrieved from the radiances measured by the Special Sensor Microwave/Imager (SSM/I) were used. We use these fluxes in this study to investigate the relationship between the SST and the air–sea fluxes. The methods for deriving the surface fluxes and the sources of data used in this study are briefly described in section 2. In section 3, the accuracy of the satellite-retrieved surface fluxes is assessed using independent measurements at the IMET buoy, RV *Moana Wave,* and RV *Wecoma* during the IOP. Section 4 investigates the spatial distributions of the surface heat budgets, as well as the relevant parameters used for deriving the surface fluxes. The impacts of the two MJOs on the surface heat budget and the contrast between the northern and southern warm pool are discussed. Section 5 examines the relation of the SST variation to the heat and momentum fluxes at the surface and the penetration of solar flux through the bottom of the ocean mixed layer. Concluding remarks are given in section 6.

2. Data sources and retrieval of surface fluxes

The daily mean surface momentum, latent heat, and sensible heat fluxes computed by Chou et al. (1997) are used in this study, which have a spatial resolution of 2.0° × 2.5° lat–long over global oceans and cover the period July 1987–December 1994. To be consistent with the spatial resolution of the radiative fluxes (to be discussed below), we linearly interpolate these fluxes onto a 1.0° × 1.0° lat–long grid in the Pacific warm pool (defined as 10°S–10°N, 135°–175°E hereafter) for the IOP.

The surface turbulent fluxes were computed using a stability-dependent aerodynamic bulk scheme of Chou (1993), which was tested against aircraft covariance fluxes measured during cold air outbreaks over the North Atlantic Ocean. Over the warm pool, the retrieved daily SSM/I wind stresses and latent heat fluxes were found to compare reasonably well with daily mean fluxes of the RV *Moana Wave* measured during the COARE IOP (Chou et al. 1997). The accuracy of the retrieved fluxes is further assessed in section 3. This scheme is similar to Fairall et al. (1996a) but without gustiness parameterization. Using the surface-layer similarity theory, the turbulent fluxes are derived from the surface-layer scaling parameters by iteratively solving the diabatic profiles of wind, temperature, and moisture. The bulk transfer coefficients are stability dependent and are

functions of wind speed, and sea–air temperature and humidity differences.

The turbulent fluxes were derived from daily mean values of SST, specific humidity, and wind speed 10 m above the sea surface, and air temperature 2 m above the sea surface. It is noted that the reference height in the bulk scheme was set to 10 m for wind speed and humidity but was set to 2 m for temperature for correctly calculating their gradients and stability (Chou et al. 1997). The 10-m wind speeds and specific humidity were derived from radiances measured by the SSM/I. The 10-m specific humidity was derived from the water vapor amount in the entire atmospheric column of Wentz (1994) and the lowest 500-m layer above the surface using the method developed by Chou et al. (1995, 1997). The latter was retrieved from the SSM/I radiances using the method of Schulz et al. (1993). The 10-m wind speeds derived by Wentz (1994) were used. Wind stress directions were taken from the surface wind directions of Atlas et al. (1996), which used the SSM/I surface wind speed of Wentz (1994).

The SSM/I data used were on board the Defense Meteorological Satellite Program (DMSP) *F10* and *F11* polar-orbiting satellites, which had ascending equatorial crossings at 1942 and 1742 LT, respectively. Each satellite had a swath of 1394 km on the earth's surface. The morning and afternoon orbits of each satellite provided approximately one observation per day in the equatorial area with increased overlapping of the two tracks poleward from the equator. The SSM/I-retrieved surface winds and water vapor amounts had an original spatial resolution of $(25\ \text{km})^2$. They were degraded to ''daily means'' and $2.0^\circ \times 2.5^\circ$ lat–long regions separately for the DMSP *F10* and *F11* satellites. The daily means indicate the values either from the morning or the afternoon orbits or the averages of both overlapping orbits. Two sets of fluxes were first computed for these two satellites separately and then averaged to form the daily mean fluxes.

The difference in the SST and the temperature at the 2-m height, $\text{SST} - T_{2m}$, used for computing the sensible heat flux was taken from the averages of 0000 and 1200 UTC analyses of the European Centre for Medium-Range Weather Forecasts (ECMWF), which had a spatial resolution of $2.0^\circ \times 2.5^\circ$ lat–long. Sea–air temperature difference is generally very small over the open ocean, except for the warm pool and midlatitudes in the winter. Small errors in the SST and T_{2m} could induce a relatively large error in $\text{SST} - T_{2m}$ if the errors are uncorrelated. The ECMWF analysis of T_{2m} is thermodynamically constrained to the SST. Thus the ECMWF $\text{SST} - T_{2m}$ was used instead of using the ECMWF T_{2m} alone. Note that the reference height for T_{2m} was set at 2 m (not 10 m) for properly computing the sensible heat flux. The SST data used for computing latent heat fluxes were taken from the National Centers for Environmental Prediction (NCEP). Daily mean SSTs were interpolated from the weekly mean values with a spatial resolution of $1.0^\circ \times 1.0^\circ$ lat–long (Reynolds and Smith 1994). The NCEP SST is derived by regressing the bulk temperature against the satellite IR radiance measurements. The daily mean bulk temperature is generally warmer than the skin temperature by ~ 0.2°C (Fairall et al. 1996b; Webster et al. 1996; Weller and Anderson 1996).

The surface radiative fluxes computed by Chou et al. (1998) are used in this study. Chou et al. (1998) derived empirical relationships between the radiances measured by the Japan's Geostationary Meteorological Satellite (GMS) and the surface radiative fluxes measured at several radiation sites during the IOP. The downward shortwave flux at the surface was computed as a function of the satellite-measured albedo in the visible channel and the solar zenith angle. When data of visible albedo were missing, the satellite-measured brightness temperature in the IR window channel was used. The downward longwave flux was computed as a function of SST, the total column water amount, and the brightness temperature in the GMS IR window channel. These empirical relationships were applied to derive the surface solar and thermal infrared fluxes in the western Pacific warm pool. The retrieved radiative fluxes originally had a spatial resolution of $(35\ \text{km})^2$ and a temporal resolution of 1 h. They were subsequently degraded to daily values with a $1.0^\circ \times 1.0^\circ$ lat–long spatial resolution. It is noted that our empirical approach to deriving the surface radiation is drastically different from the methods that use radiative transfer calculations (e.g., Chou 1994; Li and Leighton 1993; Zhang et al. 1995; Curry et al. 1999). These approaches are attractive because the physical processes that affect the radiative transfer are explicitly included. Nevertheless, the accuracy of the derived fluxes is inherently limited by inadequate information on the absorption and scattering properties of atmospheric gases and particulates (clouds and aerosols), as well as information on the temporal and spatial distributions of clouds and aerosols. One cannot with absolute certainty define either the accuracy of cloud parameters retrieved from satellite observations or the accuracy of radiative transfer models in computing fluxes in both clear and cloudy atmospheres.

To validate the satellite-retrieved surface fluxes, we use the latest version of the 7.5-min mean surface fluxes at the IMET buoy, as well as time-mean surface fluxes for three cruises of the RV *Moana Wave* and RV *Wecoma* near the IMET buoy, which were computed by Weller and Anderson (1996). Fairall et al. (1996a) derived the turbulent fluxes directly from the high-frequency temperature, humidity, and wind measurements at the RV *Moana Wave* and developed an aerodynamic bulk scheme for estimating turbulent fluxes in weak wind and convective situations. This bulk scheme was applied to derive the fluxes at IMET and RV *Wecoma*. Weller and Anderson (1996) found that the surface fluxes at the IMET buoy were in good agreement with those at the nearby *Wecoma* and *Moana Wave*. It is noted that the data used to derive the empirical relationships be-

tween the satellite radiance measurements and the surface radiative flux measurements do not include the data from IMET, *Moana Wave,* or *Wecoma.* Thus, radiative fluxes measured at these three surface platforms and those derived from the satellite-measured radiances are independent and suitable for intercomparison.

3. Collocation validation

The surface heat and momentum fluxes derived from satellite measurements are compared with that derived from observations at the IMET buoy (1.75°S, 156°E). Mean fluxes of two 1.0° × 1.0° latitude–longitude regions centered at 1.5°S, 155.5°E and 1.5°S, 156.5°E are used for the comparison with the IMET observations. The net heat flux at the surface F_{net} is defined as $F_{\text{net}} = F_{\text{SW}} - (F_{\text{LW}} + F_{\text{SH}} + F_{\text{LH}})$, where F_{SW} is the net downward solar (shortwave) flux, F_{LW} is the net upward infrared (longwave) flux, F_{SH} is the upward sensible heat flux, and F_{LH} is the latent heat flux (evaporative cooling). Figure 1 and Table 1 compare daily mean surface fluxes from the IMET buoy (solid lines) and retrievals (dashed lines, pluses, and diamonds) during the IOP. In Table 1, the daily standard deviation (std dev) error denotes the standard deviation of daily differences of fluxes between the retrieval and IMET, while the monthly and IOP std dev errors are derived with the assumption that daily errors are independent. The biases and the monthly and IOP std dev errors of the retrieved surface fluxes provide us the information on the uncertainty of the monthly and IOP mean surface heat budgets.

The net solar fluxes at the surface shown by pluses (70 days) in Fig. 1a are retrieved from the visible albedo, while those shown by diamonds (50 days) are retrieved from the IR brightness temperature when there are no albedo data available. It can be seen that the solar fluxes retrieved from the brightness temperature and the albedo have comparable accuracy. The satellite-retrieved solar flux is generally in good agreement with that measured at the IMET, except large discrepancies on some days with strong and weak solar radiation. The retrieved solar fluxes are averaged over two 1.0° × 1.0° lat–long regions containing the IMET site, whereas the area of the sky that contributes to the solar flux measured at the surface is much smaller, <10 km. Because of the difference in spatial resolution, the satellite-retrieved solar flux is less sensitive to the distribution of clouds in the vicinity of the surface site than the surface measurements. It follows that the former is smoother in time than the latter. The relatively large discrepancies at both large and small solar fluxes reflect the difference in the spatial resolutions of these two sets of fluxes rather than the satellite retrieval error. The daily mean solar flux fluctuates between 50 and 270 W m^{-2}. Table 1 shows that the retrieved F_{SW} has a mean of 196.6 W m^{-2}, a bias of 1.8 W m^{-2}, a std dev error of 32.5 W m^{-2} for the daily mean flux, and a correlation coefficient of 0.86 between the satellite retrievals and surface observations.

Figure 1b shows that the net longwave flux is much smaller than the solar flux and fluctuates within a small range between 40 and 75 W m^{-2}. Table 1 shows that the retrieved F_{LW} has a mean of 50.9 W m^{-2}, a bias of −7.1 W m^{-2}, a std dev error of 5.2 W m^{-2} for the daily mean flux, and a correlation coefficient of 0.75 between the satellite retrievals and surface observations. To investigate the relatively large bias of net longwave flux, we examine separately the upward ($F^{\uparrow}$) and downward ($F^{\downarrow}$) components of the net longwave flux, which is given by

$$F_{\text{LW}} = F^{\uparrow} - F^{\downarrow} = [\varepsilon\sigma T_s^4 + (1 - \varepsilon)F^{\downarrow}] - F^{\downarrow}, \quad (1)$$

where ε is the emissivity of sea surface, σ is Stefan–Boltzmann constant, and T_s is the SST. The emissivity is taken to be 0.97 in computing the net longwave flux at the IMET (Weller and Anderson 1996), whereas it is taken to be 1 in this study for the satellite-retrieved net longwave flux. The difference in ε only induces a difference of 2 W m^{-2} in F_{LW}. Averaged over the IOP, the NCEP SST (302.5 K) of the two comparison grid points used to compute the retrieved F_{LW} is 0.37 K higher than the skin temperature of sea surface used to compute F_{LW} at IMET, which will cause at most a difference of about 2 W m^{-2} in F_{LW}. The mean values of $F^{\uparrow}$ (475.4 W m^{-2}) and $F^{\downarrow}$ (424.4 W m^{-2}) of the satellite retrievals are larger than those at IMET by 4 and 11 W m^{-2}, respectively. Thus, the negative bias of F_{LW} is mainly due to a 2.6% overestimation of the satellite-retrieved $F^{\downarrow}$.

The satellite-retrieved and surface-measured sensible heat fluxes are shown in Fig. 1c. The retrieval significantly underestimates the peak values of the sensible heat flux. Westerly wind bursts and squalls have been observed to accompany heavy rainfall (Anderson et al. 1996; Godfrey et al. 1998). Since winds associated with heavy rain events cannot be retrieved from the SSM/I data (Wentz 1994), strong winds and, hence, peak sensible fluxes are undersampled. Other factors, such as a smaller sea–air temperature difference of the ECMWF analysis and the exclusion of the rainfall effect in the retrieval of sensible heat flux, may have contributed to the underestimation of the sensible heat flux. Although the percentage error is large, the magnitude of the bias is small. Table 1 shows that the retrieved F_{SH} has a mean of only 6.3 W m^{-2}, a bias of −2.6 W m^{-2}, and a std dev error of 1.1 W m^{-2} (0.6 W m^{-2}) for the monthly (IOP) mean sensible heat flux.

Figures 1d and 1e show that the retrieved latent heat flux and wind stress are generally in good agreement with those measured at IMET. However, for those days with a large negative bias of sensible heat flux during westerly wind bursts and squalls accompanying heavy rainfall, the retrieval also underestimates peak values of evaporative cooling and wind stress. This is mainly due to the undersampling of high winds associated with heavy rainfall as discussed above. Spatial and temporal variability may also be the cause of the underestimation of high wind speed. The daily mean turbulent fluxes at

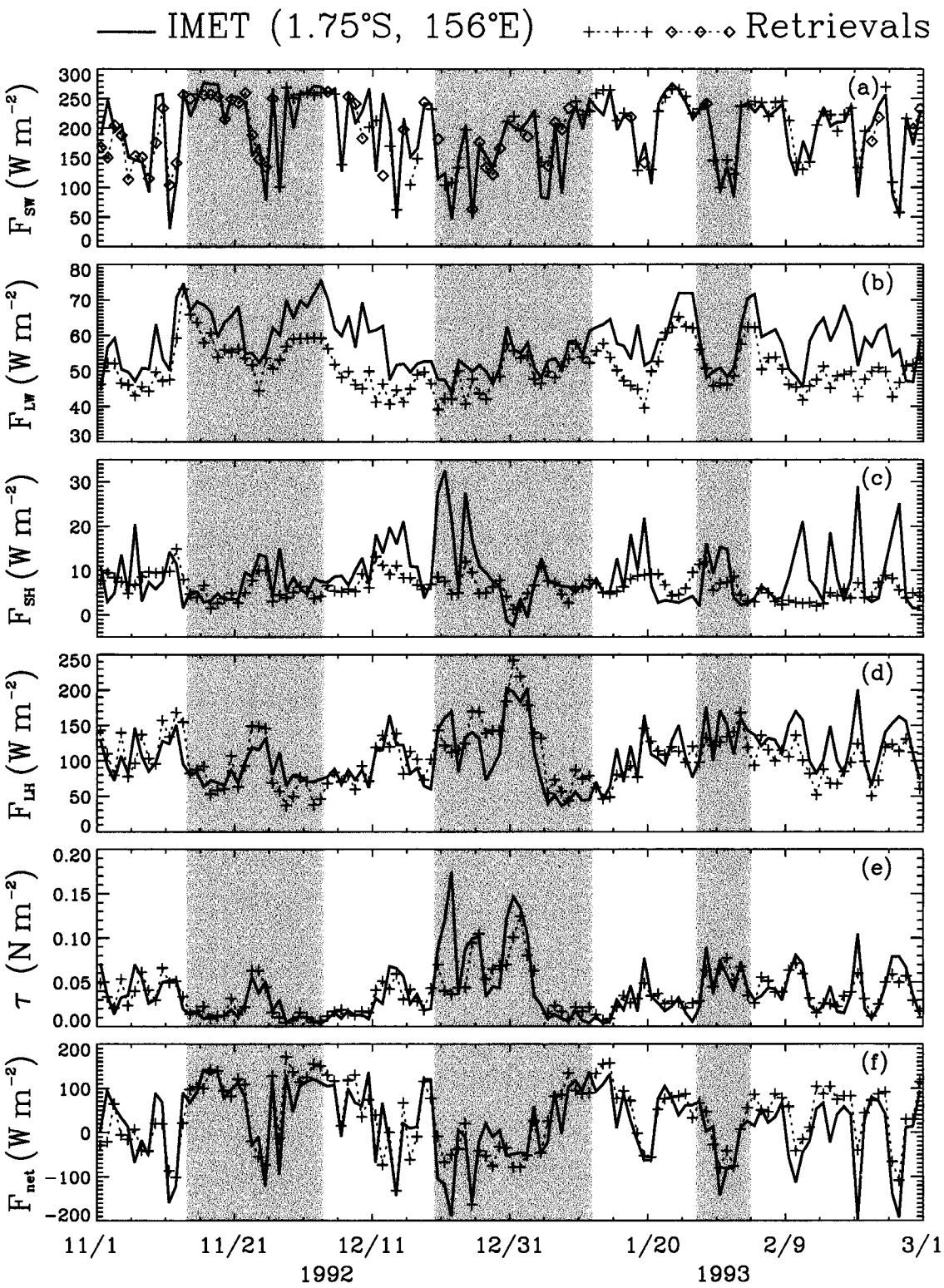

FIG. 1. Daily values at the surface for (a) net shortwave radiation, F_{SW}; (b) net longwave radiation, F_{LW}; (c) sensible heat flux, F_{SH}; (d) latent heat flux, F_{LH}; (e) wind stress, τ; and (f) net heat flux, F_{net}. Solid lines are surface measurements at IMET, while dashed lines, pluses, and diamonds are satellite retrievals.

TABLE 1. Comparison of retrieved air–sea fluxes with those measured at the IMET buoy (1.75°S, 156°E) during COARE IOP. The std dev denotes the standard deviation of retrieved fluxes from that measured at IMET. Units are W m^{-2} for heat fluxes and 10^{-4} N m^{-2} for wind stress.

			Std dev error			Correlation
	Mean	Bias	Daily	Monthly	IOP	
F_{SW}	196.6	1.8	32.5	5.9	3.0	0.86
F_{LW}	50.9	−7.1	5.2	0.9	0.5	0.75
F_{SH}	6.3	−2.6	6.1	1.1	0.6	0.40
F_{LH}	104.8	−2.4	29.1	5.3	2.7	0.71
F_{net}	34.6	13.8	48.2	8.8	4.4	0.82
τ	371	−18	210	38	19	0.78

IMET were computed from the measured 7.5-min mean local wind. However, the retrieved daily fluxes of the two finer-resolution grid points used for the comparison are interpolated from those of four coarse-resolution (2.0° × 2.5° lat–long) neighboring grid points. The retrieved daily mean fluxes are the averages of retrieved fluxes from the DMSP *F10* and *F11* satellites, which had ascending equatorial crossings at 1942 and 1742 LT, respectively. Note that the diurnal cycle cannot be resolved with only one or two SSM/I observations per day for each satellite at one location. Thus the retrieved daily mean turbulent fluxes do not include the contribution from diurnal variations. The diurnal cycle of specific humidity, wind speed, and turbulent fluxes is generally very small over the ocean (Jacob 1980; Weller and Anderson 1996; Zhang 1996). Although there is a significant diurnal cycle of SST during low winds, Ledvina et al. (1993) found that the daily mean latent heat flux derived from the daily mean temperature, humidity, and wind was only larger than the daily average of hourly fluxes by <2% over the warm pool. Table 1 shows that the latent heat flux has a mean of 104.8 W m^{-2}, a bias of −2.4 W m^{-2}, a std dev error of 29.1 W m^{-2} for the daily mean flux, and a correlation coefficient of 0.71, while the wind stress has a mean of 0.0371 N m^{-2}, a bias of −0.0018 N m^{-2}, a std dev error of 0.0210 N m^{-2} for the daily mean wind stress, and a correlation coefficient of 0.78.

The net heat flux at the surface is shown in Fig. 1f. Except for the large discrepancies on certain days with either large or small values of the net heat flux measured at IMET, which is dominated by the solar flux as mentioned above, the two sets of the net heat flux are generally in good agreement. The daily mean net heat flux fluctuates between −200 and 150 W m^{-2} for the measurements, but fluctuates between −160 and 170 W m^{-2} for the retrieval. Table 1 shows that the retrieved net heat flux has a mean of 34.6 W m^{-2}, a bias of 13.8 W m^{-2}, a std dev error of 48.2 W m^{-2} for the daily mean flux, and a correlation coefficient of 0.82.

To further validate the retrieved surface fluxes, we show in Table 2 the satellite-retrieved (Sat) surface fluxes with those from the RV *Moana Wave* (MW), RV *Wecoma* (Wec), and the IMET buoy for three observation periods of both vessels near the IMET buoy, which are shaded in Fig. 1. Weller and Anderson (1996) pointed out that leg 1 (14 November–3 December 1992) was characterized by clear skies and large spatial scales of low winds within the IFA. Leg 2 (20 December 1992–11 January 1993) started with strong westerly wind bursts across the IFA and then shifted back to clear skies with fairly uniform light winds in January 1993. Leg 3 (27 January–3 February 1993) was characterized by eastward propagating surges of westerlies and scattered clouds. There is significant variability among the three legs. The net surface heating for the ocean is positive during leg 1, as a result of small cloudiness and low wind. On the other hand, the net heating is negative for the other two legs, due to reduced solar heating and strong evaporative cooling associated with westerly wind bursts (leg 2) and squalls (leg 3). The retrieved fluxes agree reasonably well with those measured at the three surface platforms. Note that leg-averaged surface fluxes at the IMET buoy shown in Table 2 are not identical to those presented in Weller and Anderson (1996), but the difference is very small.

4. Spatial distributions of surface heat budgets

a. IOP mean

Components of the surface heat budget averaged over the COARE IOP are shown in Fig. 2, and the relevant parameters for computing surface fluxes are shown in Fig. 3. These fluxes and parameters averaged over individual months and the IOP are shown in Table 3. Figures 2a and 3a show the surface net solar flux (F_{SW}) and IR brightness temperature (T_B) for the warm pool averaged over the IOP, respectively. The spatial distri-

TABLE 2. Time-mean surface fluxes derived from satellite measurements (Sat) and from surface observations at RV *Moana Wave* (MW), RV *Wecoma* (Wec), and IMET buoy for three legs during COARE IOP. Units are W m^{-2} for heat fluxes, and 10^{-4} N m^{-2} for wind stress.

	leg 1 (14 Nov–3 Dec 1992)				leg 2 (20 Dec 1992–11 Jan 1993)				leg 3 (27 Jan–3 Feb 1993)			
	Sat	MW	IMET	Wec	Sat	MW	IMET	Wec	Sat	MW	IMET	Wec
F_{SW}	231.0	224.7	227.8	223.1	175.6	162.0	162.3	168.2	182.9	164.0	180.3	192.8
F_{LW}	56.5	62.9	64.4	62.2	48.9	52.0	52.7	55.5	51.7	53.6	55.0	59.5
F_{SH}	5.0	6.0	6.8	4.6	6.2	8.4	10.0	9.1	7.4	9.4	8.3	13.9
F_{LH}	79.4	89.7	84.6	86.1	128.1	118.8	110.1	120.3	130.1	137.6	139.3	149.6
F_{net}	90.1	66.2	71.9	70.3	−7.7	−17.2	−10.5	−16.7	−6.3	−36.6	−22.4	−30.2
τ	198	205	183	174	537	638	653	636	542	535	546	567

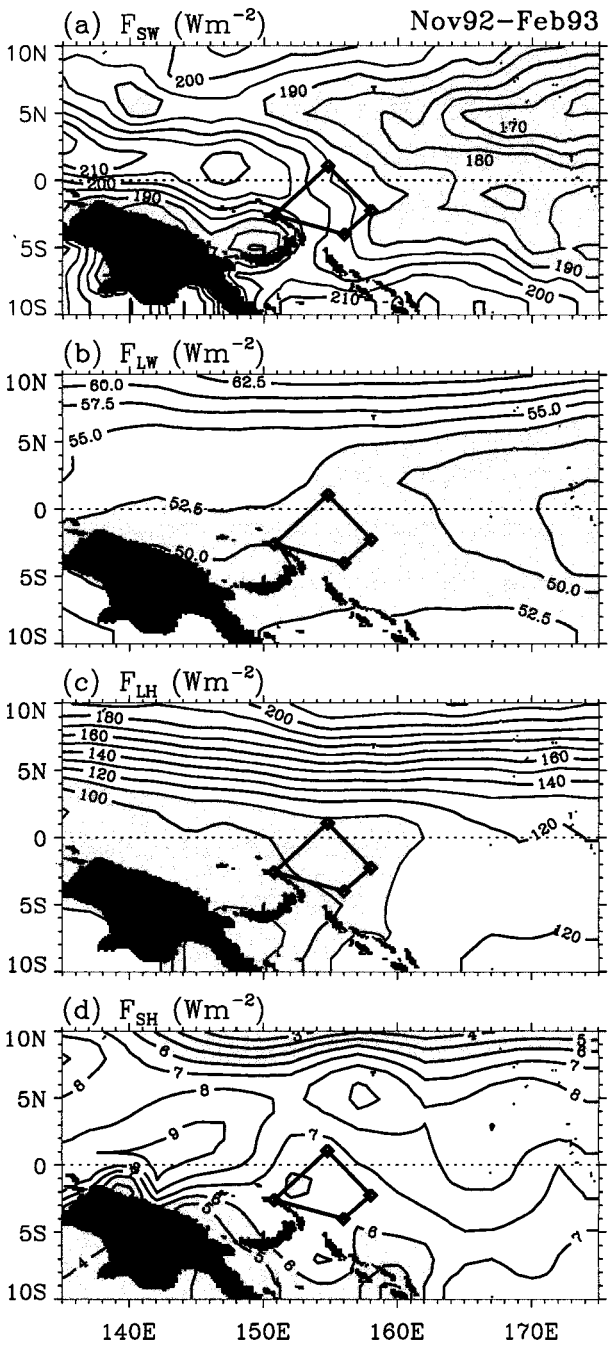

FIG. 2. Mean fields of (a) F_{SW}; (b) F_{LW}; (c) F_{LH}; and (d) F_{SH} at the surface for COARE IOP. The COARE IFA is indicated by the small box.

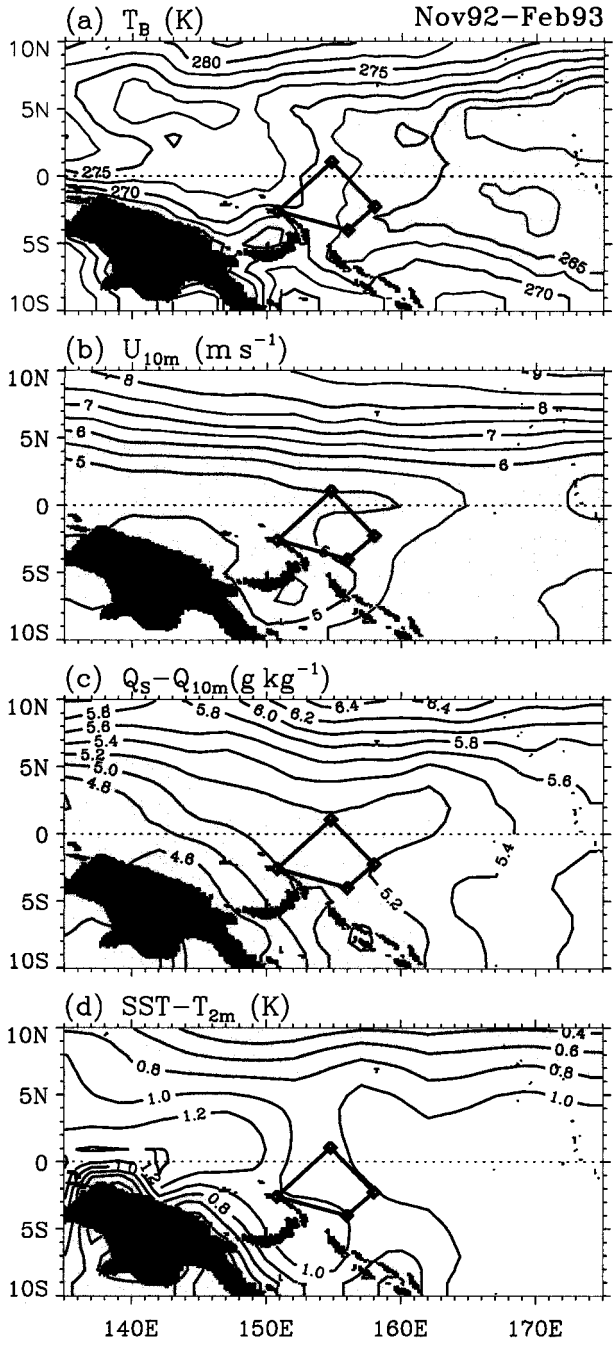

FIG. 3. Mean fields of (a) GMS IR brightness temperature, T_B; (b) 10-m surface wind speed, U_{10m}; (c) sea–air humidity difference, ($Q_s - Q_{10m}$); and (d) sea–air temperature difference, (SST $- T_{2m}$), for COARE IOP. The COARE IFA is indicated by the small box.

butions of F_{SW} and T_B are very similar, as both are dominated by clouds; strong convective activities are associated with low solar flux and IR brightness temperature. The shaded areas in the eastern warm pool and New Guinea, where $F_{SW} < 190$ W m^{-2} and $T_B < 267.5$ K, indicate regions of deep convection. There are two regions of maximum cloudiness east of 160°E and centered at 4°N and 4°S. The northern branch of the maximum cloudiness is stronger than the southern branch and extends westward across the warm pool. The minimum F_{SW} and T_B located near the date line indicates that the convection center and the upward branch of the Walker circulation shifted eastward by about 60° longitude during the COARE IOP from its normal location

TABLE 3. Monthly and IOP mean surface heat budgets and relevant parameters averaged over the Pacific warm pool (10°S–10°N, 135°–175°E).

Parameter	Units	Nov 92	Dec 92	Jan 93	Feb 93	IOP
F_{SW}	W m^{-2}	196.3	185.8	196.4	193.2	192.9
F_{LW}	W m^{-2}	53.4	53.7	54.4	52.2	53.4
F_{LH}	W m^{-2}	114.7	151.4	138.4	121.4	131.9
F_{SH}	W m^{-2}	7.3	7.6	6.7	6.0	6.9
F_{net}	W m^{-2}	20.9	−26.7	−2.9	13.7	0.7
τ	10^{-4}N m^{-2}	410	660	680	620	590
SST	°C	29.14	29.05	28.63	28.51	28.84
$\partial T_s/\partial t$	°C month^{-1}	0.30	−0.68	−0.03	−0.09	−0.14
SST − T_{2m}	K	1.1	1.0	0.9	0.8	0.9
$Q_s - Q_{10m}$	g kg^{-1}	5.4	5.9	5.4	4.7	5.4
U_{10m}	m s^{-1}	5.2	6.4	6.5	6.5	6.1
T_B	K	271.7	268.4	272.9	267.4	270.1
W	g cm^{-2}	5.1	5.0	5.0	5.1	5.0

at ~120°–130°E. The solar flux varies between 170 and 210 W m^{-2} and is ~200 W m^{-2} over the IFA. The maximum F_{SW} to the north and east of New Guinea indicates that these regions are persistently dry. It probably is caused by the descending motion induced by the strong convection over New Guinea, where topography is high and solar heating of the land surface is large. Averaged over the warm pool and the IOP, the solar heating of the ocean is 192.9 W m^{-2}.

Figure 2b shows that both the magnitude and spatial variation of the net IR cooling of the warm pool are small. The pattern of the net upward IR flux (F_{LW}) is negatively correlated with that of total precipitable water (not shown), and the increase of F_{LW} by about 10 W m^{-2} from 53 W m^{-2} at 5°N to 63 W m^{-2} at 10°N is due to a reduced column water vapor amount, W, from 5.2 cm at 5°N to 4 cm at 10°N. Clouds do not have a significant effect on the surface IR flux, as high humidity (see Table 3) makes the atmosphere very opaque to the longwave radiation.

Figures 2c, 3b, and 3c show the latent heat flux, 10-m surface wind speed (U_{10m}), and sea–air humidity difference ($Q_s - Q_{10m}$) averaged over the COARE IOP, respectively. The latent heat flux is the second largest heat budget component and is equal to 131.9 W m^{-2} when averaged over the warm pool and the IOP (Table 3). It is large mainly due to a large sea–air humidity difference. The spatial variability of latent heat flux is the largest among the budget components, varying between 90 and 220 W m^{-2}, as a larger sea–air humidity difference is coupled with a larger wind speed and vice versa. The ($Q_s - Q_{10m}$) is about 4.5–5.2 g kg^{-1} south of ~3°N and west of 160°E but increases northward to about 6.4 g kg^{-1} at 10°N, with a mean of 5.4 g kg^{-1} for the warm pool. The wind speed is about 5 m s^{-1} south of 3°N and increases northward to about 9 m s^{-1} at 10°N, with a mean of 6.1 m s^{-1} for the warm pool. This increase in wind speed reflects a northward strengthening of the northeast trade winds. Note that the mean wind speed is scalar averaged, not a vector mean of wind velocity. Thus it should be larger than the magnitude of vector mean of wind velocities over the IOP, especially over the area south of 3°–4°N where winds are weak and highly variable. The latent heat flux in the IFA is about 105 W m^{-2} and is relatively small as compared to the values of 150–220 W m^{-2} over the trade wind region in the northern warm pool.

Figures 2d and 3d show the sensible heat flux and sea–air temperature difference (SST − T_{2m}) averaged over the IOP, respectively. The sensible heat flux is the smallest heat budget component and is equal to 6.9 W m^{-2} when averaged over the warm pool and the IOP (Table 3). It is small as the sea–air temperature difference is small. Due to offset between the effects of the sea–air temperature difference and the wind speed, the spatial variability of sensible heat flux is also small (Figs. 3b,d). The (SST − T_{2m}) is about 1.0°–1.4°C in the 5°S–5°N band and decreases poleward. It has a mean of 0.9°C for the warm pool.

b. Monthly variability

Two 40–50-day MJOs associated with super cloud clusters and westerly wind bursts were observed to propagate eastward from the Indian Ocean to the central Pacific during the IOP. The super cloud clusters reduce solar heating, while the westerly wind bursts enhance evaporative cooling. Compared to the second MJO, the first MJO was associated with stronger convection, evaporative cooling, and SST cooling with a maximum impact over the southern warm pool (see section 5). The Walker circulation associated with the first and second MJOs generally had sinking motion over the southern warm pool and rising motion over Indian Ocean during November 1992 and January 1993, respectively. This situation was reversed during December 1992 and February 1993 when rising motion moved into the warm pool. The impacts of these two MJOs on the temporal and spatial variability of the surface heat budget and SST are investigated below.

It can be seen in Fig. 4 that the super cloud clusters associated with these two MJOs have a significant impact on the monthly variability of solar heating. The impact is especially large in the southern warm pool.

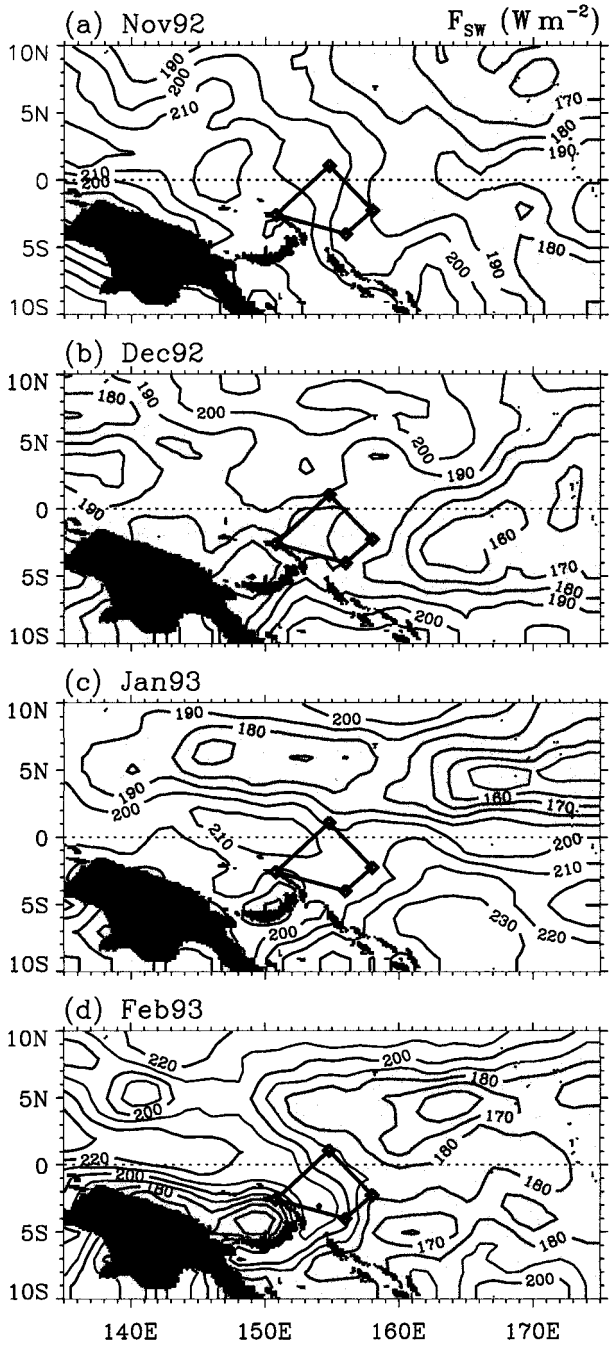

FIG. 4. Monthly mean F_{SW}. Regions of heating <190 W m^{-2} are shaded. The COARE IFA is indicated by the small box.

Figures 4a and 4c show that convection was generally suppressed with large solar heating in the southern warm pool during November 1992 and January 1993, which is affected by the sinking motions of the two MJOs. Meanwhile, the convection in the intertropical convergence zone of the northern warm pool intensified. When the super cloud clusters moved into the warm pool in December 1992 and February 1993, the surface solar heating decreased greatly in the southern warm pool, especially for the cloud band 0°–7°S in December 1992. The mean solar heating of the southern warm pool decreases by 40 W m^{-2} from November 1992 to December 1992 and by 30 W m^{-2} from January 1993 to February 1993. These results show that the super cloud clusters associated with the eastward propagating MJOs cause significant local variability of the solar heating, reaching 50 W m^{-2} on monthly scale.

The monthly and spatial variability of latent heat flux as shown in Fig. 5 is quite different from that of solar heating. In the southern warm pool, the impact of the two MJOs on the latent heat flux is smaller than the impact on the solar heating. The monthly mean latent heat flux of the southern warm pool ranges from 105.2 W m^{-2} in February 1993 to 117.3 W m^{-2} in December 1992. In the northern warm pool, on the other hand, the monthly latent heat flux increases significantly in December 1992 and January 1993, which is a result of the intensification of the northeast trade winds (not shown in the figures). In these two months, the latent heat flux is very large with the most tight gradient varying from 130 to 270 W m^{-2} across the 3°–10°N band. It increases by ~50–120 W m^{-2} from November 1992 to January 1993 due to the strengthening of the northeast trade wind coupling with increased sea–air humidity difference, which are associated with the southward shift of the trade wind belt. Averaged over the southern and northern warm pool, the monthly mean latent heat fluxes are 114.7, 151.4, 138.4, and 121.4 W m^{-2} for the four IOP months, respectively (Table 3). The large monthly variability of the warm pool mean latent heat flux is modulated by the trade winds over the northern domain of the warm pool.

Monthly variability of the net surface heat flux is shown in Fig. 6. The variability is mainly determined by solar heating in the southern warm pool and by the evaporative cooling in the northern warm pool. The IOP is a winter season in the Northern Hemisphere but is a summer season in the Southern Hemisphere. Thus, widespread net heating occurs in the southern warm pool except for the cooling in the regions east of 160°E and north and south of New Guinea during the first MJO in December 1992. Net cooling is confined nearly entirely to the northern warm pool. The strong cooling reaching a magnitude >100 W m^{-2} occurs near the northern edge of the warm pool in December 1992 and January 1993. This strong cooling is mainly due to the enhanced evaporative cooling caused by the strengthening of the northeast trade wind associated with the southward shift of the trade wind belt as discussed above. Averaged over the warm pool, monthly mean net heat fluxes are 20.9, -26.7, -2.9, and 13.7 W m^{-2} for November 1992, December 1992, January 1993, and February 1993, respectively (Table 3). Weighted by the number of days in each month, the mean heating of the warm pool during the IOP is only 0.7 W m^{-2}.

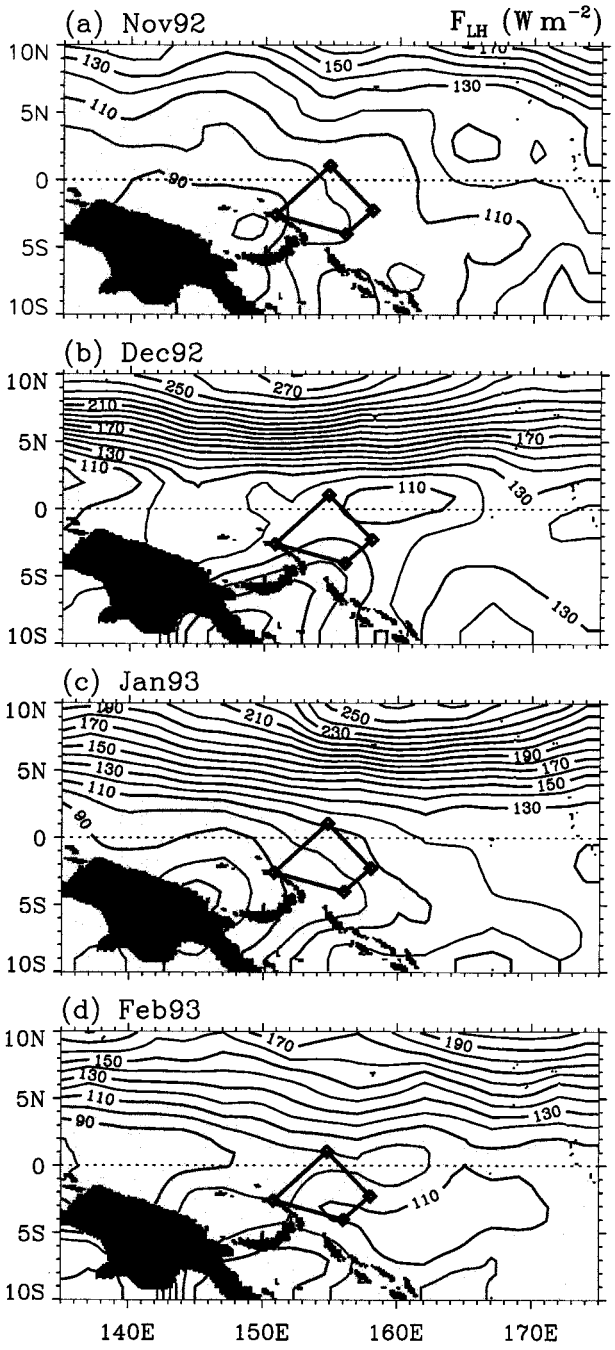

FIG. 5. Monthly mean F_{LH}. Regions of cooling <110 W m^{-2} are shaded. The COARE IFA is indicated by the small box.

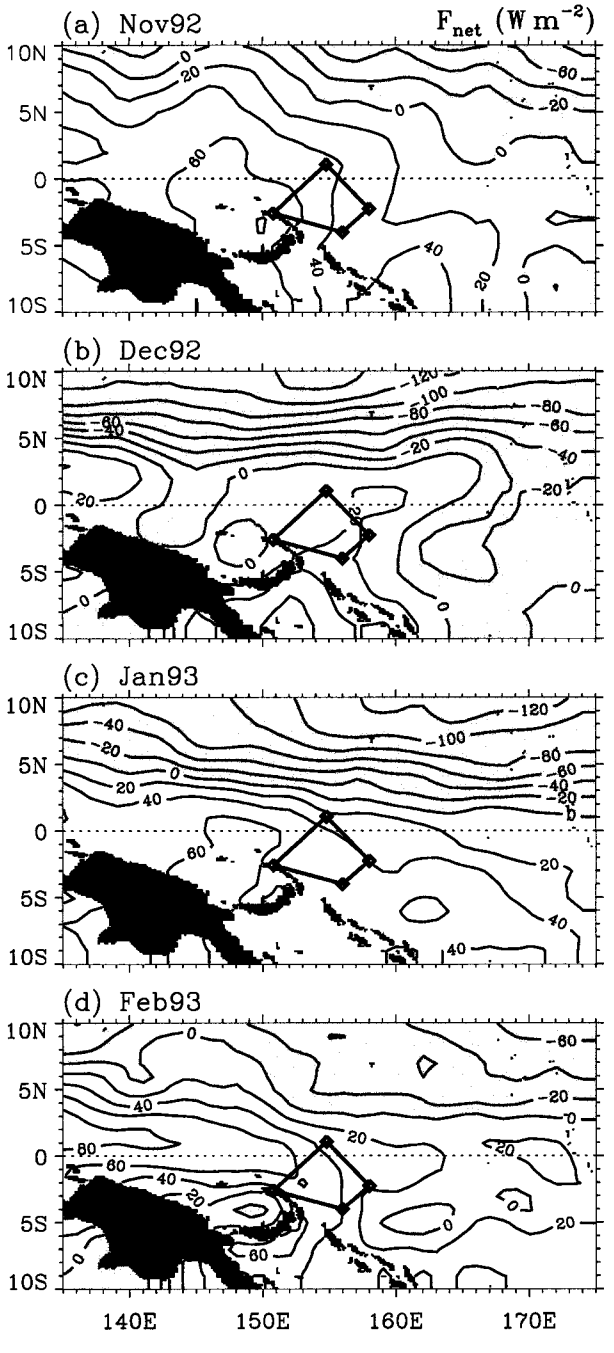

FIG. 6. Monthly mean F_{net}. Regions of cooling are shaded. The COARE IFA is indicated by the small box.

5. Relation of SST variation to surface fluxes

a. Spatial variability

The rate of change in the temperature of the ocean mixed layer or the SST is determined by the heat convergence and the depth of the mixed layer. The former involves the net heat flux at the surface and advection of heat by ocean currents, as well as the transmission of solar radiation and the entrainment of cold water through the bottom of the mixed layer. The western equatorial Pacific is characterized by frequent heavy rainfall and weak mean winds with highly intermittent westerly wind bursts. The mixed layer with constant density has been observed to be generally very shallow. Beneath it is a nearly isothermal barrier layer where density increases with depth due to salinity that inhibits the entrainment of cold water from the thermocline into

the mixed layer except during strong westerly wind bursts (Lukas and Lindstrom 1991; Sprintall and Tomczak 1992; Anderson et al. 1996; Ando and McPhaden 1997). The horizontal advection of heat in the warm pool has been found to be generally small due to weak SST gradients and currents (Niiler and Stevenson 1982; Enfield 1986; Godfrey and Lindstrom 1989).

Assuming that the advection of heat and entrainment of cold water are negligible, the heat budget of the mixed layer may be written as (Anderson et al. 1996)

$$h\rho C_p(\partial T_s/\partial t) = F_{\text{net}} - f(h)F_{\text{SW}}, \qquad (2)$$

where h is the mixed layer depth, ρ is the density of sea water, C_p is the heat capacity of sea water at constant pressure, $\partial T_s/\partial t$ is the rate of change in the SST, and $f(h)$ is the fraction of F_{SW} penetrating through the depth h. Using the water ''type 1A'' data of Jerlov (1968), Paulson and Simpson (1977) derived $f(h)$ as

$$f(h) = \gamma e^{-\alpha h} + (1 - \gamma)e^{-\beta h}, \qquad (3)$$

where $\gamma = 0.38$, $\alpha = 0.05$ m^{-1}, and $\beta = 1.67$ m^{-1}. In (3), the solar spectrum at the sea surface is divided into two groups, one corresponding to the visible region and the other corresponding to the near infrared region. The weights of the energy contained in these two spectral regions are γ and $1 - \gamma$, and the absorption coefficients of sea water are α and β, respectively. Siegel et al. (1995) studied the solar radiation penetrating at various depths in the upper ocean using the measurements made from the RV *Vickers* during the COARE IOP. The net solar fluxes given in their Table 2 fit very well with (3) if the absorption coefficient α changes slightly from 0.05 to 0.045 m^{-1}.

Using daily values of $\partial T_s/\partial t$, F_{net}, and F_{SW}, we solve (2) and (3) for h and $f(h)F_{\text{SW}}$. Because (2) and (3) are simplified nonlinear equations and because there are uncertainties in $\partial T_s/\partial t$, F_{net}, F_{SW}, and α, we cannot always find solutions for h and $f(h)F_{\text{SW}}$. This is especially so in most of the regions north of 5°N during 11–21 January 1993. In the case that h and $f(h)F_{\text{SW}}$ cannot be found for a given day, they are spatially interpolated from that of neighboring regions. The solutions to (2) and (3) can only be considered as approximations to the mixed layer depth and the solar flux reaching the bottom of the mixed layer. Nevertheless, their spatial and temporal distributions are useful for studying the relation between SST, wind stress, and mixed layer heat budgets.

The spatial distributions of F_{net} and $\partial T_s/\partial t$ averaged over the IOP are shown in Figs. 7a and 7b, respectively. As expected, the ocean gains heat in the summer (southern) hemisphere while loses heat in the winter (northern) hemisphere, with the net heat flux ranging from -80 W m^{-2} in the northeastern section of the warm pool to 40 W m^{-2} north of New Guinea. Averaged over the warm pool, the net heating is only 0.7 W m^{-2}. This result is consistent with the studies of Godfrey and Lindstrom (1989) and Godfrey et al. (1991) that the mean surface net heat flux into the warm pool is small (<10 W m^{-2}). On the other hand, Fig. 7b shows that, except near the southern edge, the warm pool cools during the IOP. The cooling increases northward and reaches a maximum >0.5°C month^{-1}. Averaged over the warm pool, the SST cools at a rate of 0.14°C month^{-1}, which does not agree with a surface heating of 0.7 W m^{-2}. The discrepancy is particularly large in the southern warm pool. For example, the net surface heat flux north of New Guinea has a maximum >40 W m^{-2}, but the SST cools at a rate of 0.3°C month^{-1}. This is an indication that much of the solar flux incident at the surface penetrates through the bottom of the mixed layer and is not available for heating the layer.

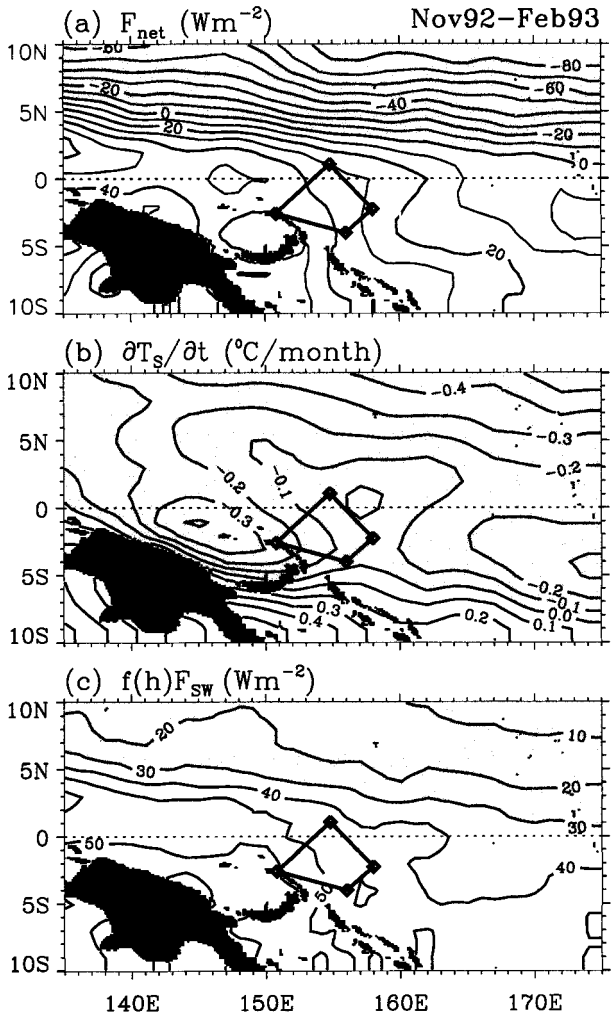

FIG. 7. Mean fields of (a) F_{net}; (b) rate of SST change, $\partial T_s/\partial t$; and (c) penetration of solar radiation through bottom of mixed layer, $f(h)F_{\text{SW}}$, for COARE IOP. The COARE IFA is indicated by the small box.

Figure 7c shows the estimated solar flux penetrating through bottom of the mixed layer, $f(h)F_{\text{SW}}$, averaged over the IOP. The solar radiation lost through the bottom of the mixed layer is ~26 W m^{-2} for the northern warm pool and ~45 W m^{-2} for the southern warm pool. The

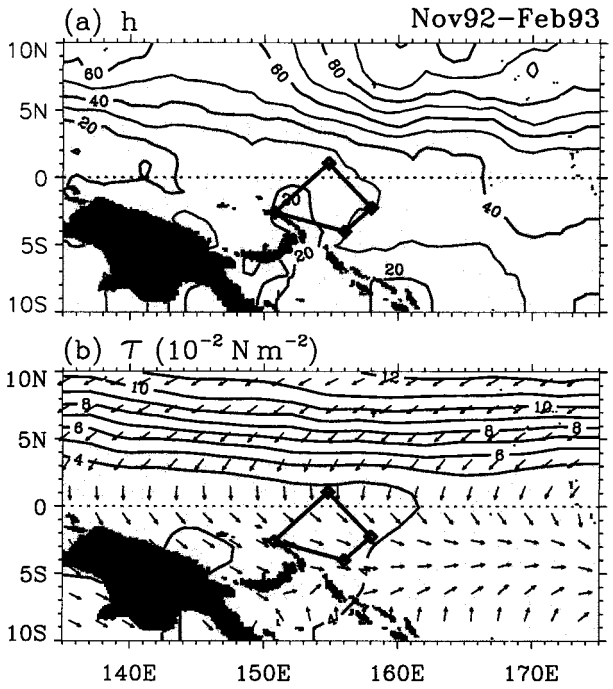

FIG. 8. Mean fields of (a) h, and (b) τ for COARE IOP. Arrows are mean wind stress directions. The COARE IFA is indicated by the small box. The unit of h is meter.

domain-averaged value of 35 W m^{-2} is significantly larger than the net surface heat flux of 0.7 W m^{-2}. Thus, the cooling of SST in the warm pool during the IOP is primarily due to this loss of solar radiation, although the infrequent westerly wind bursts may deepen the mixed layer to the top of the thermocline and entrain cold water from below.

The mixed layer depth h and the scalar-averaged wind stress τ averaged over the IOP are shown in Figs. 8a and 8b, respectively. The mean wind stress directions are also shown in Fig. 8b. The pattern of h follows closely that of τ, consistent with the finding of Ando and McPhaden (1997). In the northern warm pool, h and τ increase northward. In the southern warm pool, h and τ are rather uniform. The estimated h is $\sim$10–100 m over the warm pool, which compares reasonably well with the mean mixed layer depth of 40–70 m observed by Ando and McPhaden (1997). In the vicinity of the IMET buoy, the estimated h is 24 m, which compares with the mean mixed layer depth of 15–17 m measured and modeled during the IOP (Anderson et al. 1996; Lagerloef et al. 1998). Averaged over the southern warm pool, the estimated h is 28 m, which compares well with the mean mixed layer depth of 29 m measured by Lukas and Lindstrom (1991) in the equatorial western Pacific.

The similarity between h and τ indicates that the mixed layer in the warm pool is mainly driven by winds. Winds supply turbulent kinetic energy for mixing and thus deepen the mixed layer. On the other hand, both positive downward heat and freshwater (precipitation minus evaporation) fluxes at the surface reduce the density of water and supply a positive surface buoyancy flux, which inhibits mixing and reduces the depth of mixed layer. For the case of positive surface buoyancy forcing with insignificant entrainment cooling, the mixed layer depth is proportional to u_*^3 and inversely proportional to the surface buoyancy flux (Niiler and Kraus 1977; Anderson et al. 1996), where u_* is the friction velocity proportional to the square root of the wind stress. Anderson et al. (1996) found that the surface buoyancy forcing on the mixed layer of the warm pool was generally positive and varied little on timescales longer than 2 days. It is a result of the fact that negative buoyancy forcing, due to surface cooling caused by westerly wind bursts and squall events, is accompanied by positive buoyancy forcing, due to positive freshwater flux from heavy rain. The near-constant positive surface buoyancy forcing suggests that the mixed layer depth is dependent primarily on the wind forcing.

b. Temporal variability

We have analyzed the two MJOs using the time–longitude sections of daily IR brightness temperature and surface zonal wind averaged over the 0°–10°S band from 80°E to 160°W for the COARE IOP (not shown). There were two super cloud clusters with $T_B < 253$ K and two wind bursts with 10-m westerly zonal wind of 5–12 m s^{-1}. The super cloud clusters and the westerly wind bursts covered a zonal width of 20°–40° longitude and were associated with two MJOs propagating eastward with a speed of 3.6 m s^{-1} from the Indian Ocean to the central Pacific. The two westerly wind bursts moved through the southern warm pool during the periods from 20 December 1992 to 5 January 1993 and from 28 January 1993 to 28 February 1993 with the super cloud clusters right ahead of them. To further study the impacts of these two MJOs on the surface heat budgets and SST evolution, we have analyzed the time series of 5-day running means of SST, surface and mixed layer heat budgets, scalar-averaged wind stress, and mixed layer depth averaged over the southern and northern warm pool, separately. The results are shown in Fig. 9 for the former and Fig. 10 for the latter.

Figure 9a shows that the SST in the southern warm pool is modulated by the two MJOs, with the maximum SST near 9 December 1992 and 20 January 1993. During the period from 5 November 1992 to 9 December 1992, the ascending branch of the first MJO was over the Indian ocean while the southern warm pool was in the dry descending phase. Figures 9b, and 9c show that the sky was generally clear with little cloud and that easterly winds are weak as indicated by the large F_{SW} and the small F_{LH} and τ. Convection intensified from 10 December 1992 to 24 December 1992 as the super cloud cluster and wet phase of the first MJO moved into

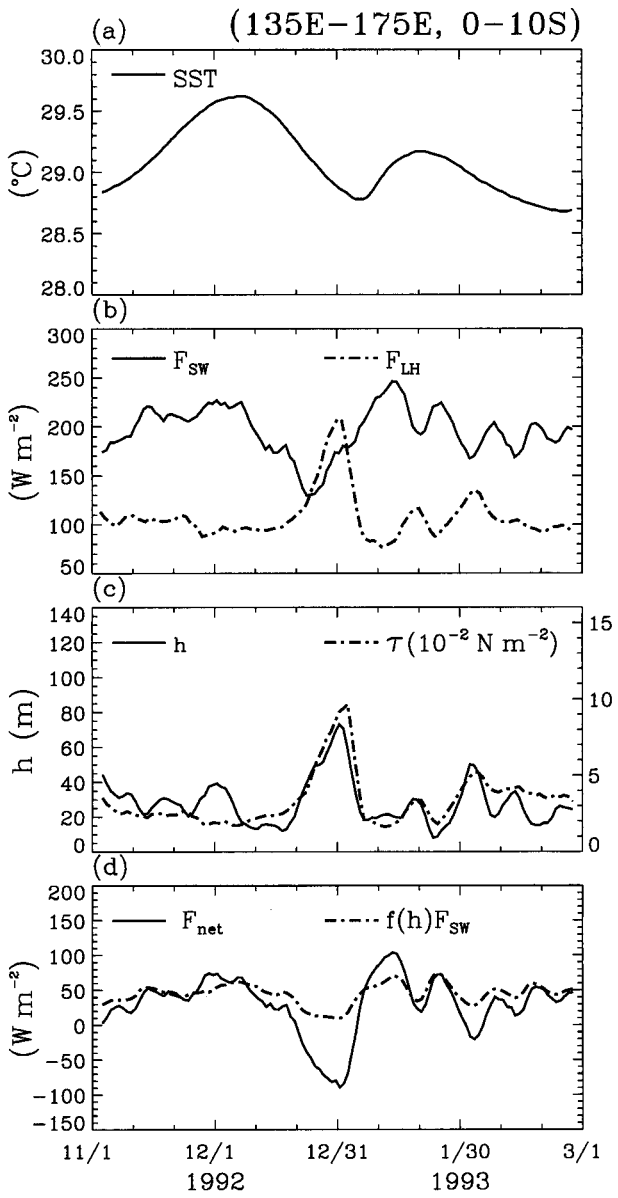

FIG. 9. Time series of 5-day running mean (a) SST; (b) F_{SW}, and F_{LH}; (c) h, and τ; and (d) F_{net}, and solar radiation penetrating through bottom of mixed layer, $f(h)F_{SW}$, averaged over the region 0°–10°S and 135°–175°E.

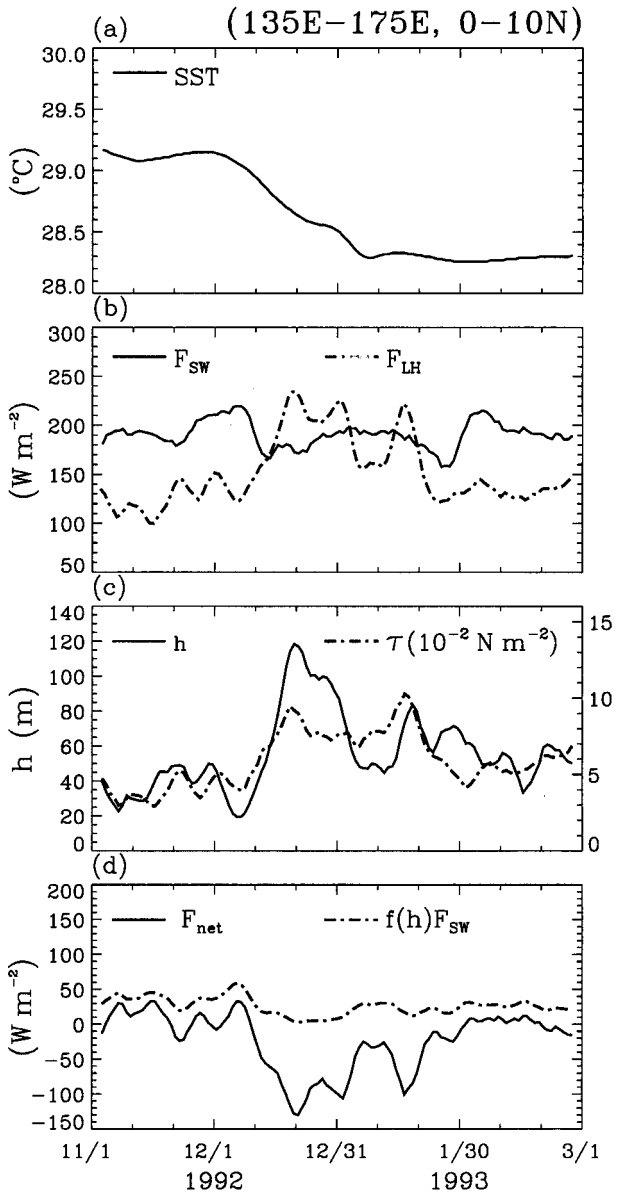

FIG. 10. Same as Fig. 9, except for the region 0°–10°N and 135°–175°E.

the southern warm pool from the Indian Ocean as indicated by the decreasing F_{SW}, while F_{LH} and τ associated with weak convergent winds remained small. Convection weakened from 25 December 1992 to 5 January 1993 as the super cloud cluster departed from the warm pool to the central Pacific and induced the strongest westerly wind burst, as indicated by the maximum F_{LH} and τ, with sinking motion over the southern warm pool. The maximum westerly wind (or F_{LH}) was induced by the strong convection centered around the date line where the SST is very high. Thus, in the southern warm pool, the maximum westerly wind (or maximum F_{LH}) lagged the most intense convection (or minimum F_{SW}) by ~9 days. The maximum westerly wind lagged the warmest SST by 25 days and led the coldest SST by 5 days. These phase relationships are in good agreement with previous findings based on the observations from the IMET buoy (Lin and Johnson 1996; Lau and Sui 1997), as the first MJO is spatially very coherent.

The second MJO started with dry descending phase on 6 January 1993 but lasted for only a short period until about 27 January 1993. It is noted that the minimum F_{SW} and the maximum F_{LH} on 20 January 1993 are not related to the westerly wind burst but are caused by the relatively strong southeasterly trade wind. Both

the westerly wind burst and strong convection reached the maximum strength near 4 February 1993. The strength is weaker for the second MJO than the first MJO, likely due to a cooler SST. The second peak of SST in the southern warm pool is 0.4°C cooler than the first peak, due to a shorter duration of heating. The convection associated with the second super cloud cluster is thus weaker than the first one, as less water vapor associated with a cooler SST is available to form clouds. The reduction of the 5-day mean solar heating is only 50 W m^{-2} for the second super cloud cluster but is 100 W m^{-2} for the first super cloud cluster. The weaker second super cloud cluster in turn induces a weaker second westerly wind burst, which enhances the 5-day mean evaporating cooling by only 50 W m^{-2}, rather than 100 W m^{-2} by the first wind burst. Also different from the first MJO, there is no time lag between the strong westerly winds and large cloud amount during the second MJO. This results from the absence of strong westerly winds associated with convection in the central Pacific, due to a cooler SST and weaker convection as compared to the first MJO.

Figure 9c shows that the temporal variability of the mixed layer depth derived from (2) and (3) follows closely that of the wind stress. The mixed layer in the southern warm pool is generally very shallow, ~20 m, and deepens during the westerly wind bursts, reaching ~70 m. It has a mean of 28 m during the IOP. Figure 9d shows that the estimated solar radiation penetrating through the bottom of the mixed layer, $f(h)F_{SW}$, is significant in the southern warm pool as the mixed layer is shallow. As a result, the rate of change in the SST does not follow the net surface heat flux, F_{net}, except during the westerly wind burst of the first MJO (Figs. 9a,d). Thus the penetration of solar radiation through the mixed layer in the southern warm pool is important to the mixed layer heat budget and SST variation, in agreement with the conclusions of Anderson et al. (1996) and Sui et al. (1997).

The SST, surface fluxes, and mixed layer heat budgets shown in Fig. 10 for the northern warm pool present a very different picture from that of the southern warm pool. The northeasterly trade wind intensified in the middle period of the IOP, 11 December 1992–21 January 1993 (Fig. 10c). This seasonal intensification of the trade wind induces a large increase in F_{LH} (110 W m^{-2}), but only a slight decrease in F_{SW} (Fig. 10b). As a result, the net surface heating F_{net} decreases significantly with a minimum of -130 W m^{-2} (Fig. 10d). Before and after this period, F_{net} is close to zero. Consistent with F_{net}, the SST decreases during this period except 11–21 January 1993 and remains nearly unchanged before and after this period (Fig. 10a). This is a result of deep mixed layer in the northern warm pool and, hence, the small solar radiation penetrating through the bottom of the layer (Figs. 10c,d). During 11–21 January 1993, the solutions of h and $f(h)F_{SW}$ are missing in most of the regions north of 5°N. This is probably because the fact that the mixed layer heat budget equation (2) neglects the advection due to the North Equatorial Countercurrent in the region, together with the uncertainties in the input parameters $\partial T_s/\partial t$, F_{net}, F_{SW}, and α.

6. Concluding remarks

Using satellite radiance measurements, the heat and momentum fluxes at the surface of the Pacific warm pool have been derived for the COARE Intensive Observing Period, November 1992–February 1993. Daily values of the satellite-retrieved fluxes in the vicinity of the IMET buoy during the IOP are generally in good agreement with that of the buoy measurements. Averaged over the three time legs of the RVs *Moana Wave* and *Wecoma* observations near the IMET buoy, there is also good agreement between the satellite-retrieved fluxes and the fluxes measured at the IMET buoy and the two vessels. These results show that the retrieved surface fluxes can be used to study the surface heat budget over the warm pool.

The characteristics of surface heat and momentum fluxes during the IOP are very different between the southern warm pool and the northern warm pool. In the southern warm pool, winds are generally weak except during short episodes of westerly wind bursts. As a result, the solar heating at the surface is much larger than the evaporative cooling. Averaged over the southern warm pool and the IOP, it is 196 W m^{-2} for the solar heating and only 108 W m^{-2} for the evaporative cooling, and the impact of the two MJOs on the surface solar flux is significantly larger than the impact on the latent heat flux. The monthly variation of the net surface heat flux is dominated by the solar radiation. Associated with the weak surface winds, the ocean mixed layer in the southern warm pool is shallow with an estimated mean depth of ~28 m. Because of the shallow mixed layer, a significant amount of solar radiation incident at the surface penetrates through the bottom of the mixed layer (~45 W m^{-2}), and the rate of change in the surface temperature does not follow the net surface heat flux.

In the northern warm pool, the northeasterly trade wind averaged over the IOP is strong with a maximum >8 m s^{-1}. The domain-averaged latent heat flux during the IOP is 148 W m^{-2}, which is much larger than the latent heat flux in the southern warm pool. The monthly variation of the net surface heat flux is dominated by the latent heat flux that is, in turn, dominated by the seasonal change in the strength of the northeasterly trade wind. Because of the strong surface wind, the mean mixed layer is deep, estimated to be ~56 m, and the solar radiation penetrating through the bottom of the mixed layer is small. The rate of change in SST during the IOP follows closely the net surface heat flux, except during 11–21 January 1993. Also different from the southern warm pool, the MJOs does not have a clear

impact on the surface heat budgets of the northern warm pool.

Averaged over the IOP, ocean gains heat in the summer (southern) hemisphere while it loses heat in the winter (northern) hemisphere, with the net heat flux ranging from -80 W m^{-2} in the northeastern section of the warm pool to 40 W m^{-2} north of New Guinea. Averaged over the warm pool and IOP, the net heating is only 0.7 W m^{-2}. This result is consistent with the studies of Godfrey and Lindstrom (1989) and Godfrey et al. (1991) that the mean surface net heat flux into the warm pool is small.

Surface heat flux is very sensitive to the sea surface temperature. Webster et al. (1996) have shown that a change in the surface skin temperature of 1°C would induce a change of $\sim$27 W m^{-2} in the net surface heat flux if other parameters are fixed. The NCEP provides only the weekly mean SST derived from National Oceanic and Atmospheric Administration (NOAA) Advanced Very High Resolution Radiometer (AVHRR) thermal infrared radiance measurements. Satellite measurements in thermal IR channels can only provide surface information when there are no clouds in the satellite field of view. Thus, the retrieved SST is biased to the SST when the sky is clear. Since the radiance measurements are regressed against the buoy temperature measurements that are representative of the temperature at the level 0.5 m below the surface, the NCEP SST is not exactly the skin temperature. The skin temperature is usually 0.2°C cooler than the temperature at 0.5 m below the surface (Webster et al. 1996). Furthermore, the NOAA satellites are polar orbiting. They scan the same spot on the earth roughly twice a day at fixed local time, and the retrieved SST may not be representative of the daily mean SST, especially during clear-sky situations when the SST is retrieved. The impact of these SST uncertainties on the results presented in this study is difficult to assess.

The mixed layer depth is estimated using a simple heat budget equation that neglects the horizontal advection and vertical entrainment of heat. The uncertainties in the retrieved surface heat budgets, SST tendency, and the solar radiation absorption coefficient of sea water, as well as the neglect of the advection and entrainment, are expected to affect the estimation of the mixed layer depth. Nevertheless, the estimated mixed layer depth is in general agreement with other studies, and conclusions of this study are not expected to be much affected by these uncertainties and simplifications.

Acknowledgments. This study was supported by the TRMM Program and Radiation Research Program, NASA/Office of Earth Science. Daily SSM/I air–sea turbulent fluxes were processed by C.-L. Shie and J. Ardizzone. The SSM/I data of total precipitable water, wind speeds, and antenna temperatures were provided by F. Wentz. The NCEP SSTs were provided by R. W. Reynolds. The sea–air temperature differences were provided by the ECMWF. The 7.5-min mean fluxes of IMET buoy and lag-averaged fluxes of RVs *Moana Wave* and *Wecoma* were computed by R. A. Weller and S. P. Anderson. The GMS albedo and brightness temperature were compiled by P. Flament and R. Bernstein. Helpful comments from two anonymous reviewers are greatly appreciated.

REFERENCES

Anderson, S. P., R. A. Weller, and R. B. Lukas, 1996: Surface buoyancy forcing and the mixed layer of the western Pacific warm pool: Observations and one-dimensional model results. *J. Climate,* **9,** 3056–3085.

Ando, K., and M. J. McPhaden, 1997: Variability of surface layer hydrography in the tropical Pacific Ocean. *J. Geophys. Res.,* **102,** 23 063–23 078.

Atlas, R., R. N. Hoffman, S. C. Bloom, J. C. Jusem, and J. Ardizzone, 1996: A multiyear global surface wind velocity dataset using SSM/I wind observations. *Bull. Amer. Meteor. Soc.,* **77,** 869–882.

Chou, M.-D., 1994: Radiation budgets in the western tropical Pacific. *J. Climate,* **7,** 1958–1971.

——, W. Zhao, and S.-H. Chou, 1998: Radiation budgets and cloud radiative forcing in the Pacific warm pool during TOGA COARE. *J. Geophys. Res.,* **103,** 16 967–16 977.

Chou, S.-H., 1993: A comparison of airborne eddy correlation and bulk aerodynamic methods for ocean–air turbulent fluxes during cold-air outbreaks. *Bound.-Layer Meteor.,* **64,** 75–100.

——, R. M. Atlas, C.-L. Shie, and J. Ardizzone, 1995: Estimates of surface humidity and latent heat fluxes over oceans from SSM/I data. *Mon. Wea. Rev.,* **123,** 2405–2425.

——, C.-L. Shie, R. M. Atlas, and J. Ardizzone, 1997: Air–sea fluxes retrieved from Special Sensor Microwave Imager data. *J. Geophys. Res.,* **102,** 12 705–12 726.

Clayson, C. A., and J. A. Curry, 1996: Determination of surface turbulent fluxes for the Tropical Ocean-Global Atmosphere Coupled Ocean–Atmosphere Response Experiment: Comparison of satellite retrievals and in situ measurements. *J. Geophys. Res.,* **101,** 28 515–28 528.

Cronin, M. F., and M. J. McPhaden, 1997: The upper ocean heat balance in the western equatorial Pacific during September–December 1992. *J. Geophys. Res.,* **102,** 8533–8554.

Curry, J. A., C. A. Clayson, W. B. Rossow, R. Reeder, Y.-C. Zhang, P. J. Webster, G. Liu, and R.-S. Sheu, 1999: High-resolution satellite-derived dataset of the surface fluxes of heat, freshwater, and momentum for the TOGA COARE IOP. *Bull. Amer. Meteor. Soc.,* **80,** 2059–2080.

Enfield, D. B., 1986: Zonal and seasonal variations of the near-surface heat balance of the equatorial Pacific Ocean. *J. Phys. Oceanogr.,* **16,** 1038–1054.

Fairall, C. W., E. F. Bradley, D. P. Rogers, J. B. Edson, and G. S. Young, 1996a: Bulk parameterization of air–sea fluxes for Tropical Ocean Global Atmosphere Coupled Ocean–Atmosphere Response Experiment. *J. Geophys. Res.,* **101,** 3747–3764.

——, ——, J. S. Godfrey, J. B. Edson, G. S. Young, and G. A. Wick, 1996b: Cool-skin and warm-layer effects on sea surface temperature. *J. Geophys. Res.,* **101,** 1295–1308.

Feng, M., P. Hacker, and R. Lukas, 1998: Upper ocean heat and salt balances in response to a westerly wind burst in the western equatorial Pacific during TOGA COARE. *J. Geophys. Res.,* **103,** 10 289–10 311.

Godfrey, J. S., and E. J. Lindstrom, 1989: On the heat budget of the equatorial west Pacific surface mixed layer. *J. Geophys. Res.,* **94,** 8007–8017.

——, M. Nunez, E. F. Bradley, P. A. Coppin, and E. J. Lindstrom, 1991: On the net surface heat flux into the western equatorial Pacific. *J. Geophys. Res.,* **96,** 3343–3357.

——, R. A. House Jr., R. H. Johnson, R. Lukas, J.-L. Redelsperger, A. Sumi, and R. Weller, 1998: Coupled Ocean–Atmosphere Response Experiment (COARE): An interim report. *J. Geophys. Res.,* **103,** 14 395–14 450.

Gutzler, D., G. N. Kiladis, G. A. Meehl, K. M. Weickman, and M. Wheeler, 1994: The global climate of December 1992–February 1993. Part II: Large-scale variability across the tropical western Pacific during TOGA COARE. *J. Climate,* **7,** 1606–1622.

Jacob, C. A., 1980: Mean diurnal and shorter period variations in the air–sea fluxes and related parameters during GATE. *Deep.-Sea Res.,* **26** (Suppl. I), 65–98.

Jerlov, N. G., 1968: *Optical Oceanography.* Elsevier, 194 pp.

Lageloef, G. S., R. Lukas, R. A. Weller, and S. P. Anderson, 1998: Pacific warm pool temperature regulation during TOGA COARE: Upper ocean feedback. *J. Climate,* **11,** 2297–2309.

Lau, K.-M., and C.-H. Sui, 1997: Mechanism of short-term sea surface temperature regulation: Observations during TOGA COARE. *J. Climate,* **10,** 465–472.

Ledvina, D. V., G. S. Young, R. A. Miller, and C. W. Fairall, 1993: The effect of averaging on bulk estimates of heat and momentum fluxes for the tropical western Pacific Ocean. *J. Geophys. Res.,* **98,** 20 211–20 217.

Lewis, M. R., M.-E. Carr, G. C. Feldman, W. Esaias, and C. McClain, 1990: Influence of penetrating solar radiation on the heat budget of the equatorial Pacific Ocean. *Nature,* **347,** 543–545.

Li, Z., and H. G. Leighton, 1993: Estimation of SW flux absorbed at the surface from TOA reflected flux. *J. Climate,* **6,** 317–330.

Lin, X., and R. H. Johnson, 1996: Kinematic and thermodynamic characteristics of the flow over the western Pacific warm pool during TOGA COARE. *J. Atmos Sci.,* **53,** 695–715.

Lukas, R., and E. Lindstrom, 1991: The mixed layer of the western equatorial Pacific Ocean. *J. Geophys. Res.,* **96** (Suppl.), 3343–3357.

Madden, R. A., and P. R. Julian, 1994: Observations of the 40–50 day tropical oscillation—A review. *Mon. Wea. Rev.,* **122,** 814–837.

Niiler, P. P., and E. B. Kraus, 1977: One-dimensional models of the upper ocean. *Modeling and Prediction of the Upper Layers of the Ocean,* E. B. Kraus, Ed., Pergamon Press, 142–172.

——, and J. Stevenson, 1982: The heat budget of tropical warm pools. *J. Mar. Res.,* **40** (Suppl.), 465–480.

Paulson, C. A., and J. J. Simpson, 1977: Irradiance measurements in the upper ocean. *J. Phys. Oceanogr.,* **7,** 1722–1735.

Ralph, E. A., K. Bi, P. P. Niiler, and Y. du Penhoat, 1997: A Lagrangian description of the western equatorial Pacific response to the wind burst of December 1992. *J. Climate,* **10,** 1706–1721.

Reynolds, R. W., and T. M. Smith, 1994: Improved global sea surface temperature analyses. *J. Climate,* **7,** 929–948.

Schluessel, P., L. Schanz, and G. Englisch, 1995: Retrieval of latent heat flux and longwave irradiance at the sea surface from SSM/I and AVHRR measurements. *Adv. Space Res.,* **16,** 107–116.

Schulz, J., P. Schluessel, and H. Grassl, 1993: Water vapor in the atmospheric boundary layer over oceans from SSM/I measurements. *Int. J. Remote Sens.,* **14,** 2773–2789.

——, J. Meywerk, S. Ewald, and P. Schluessel, 1997: Evaluation of satellite-derived latent heat fluxes. *J. Climate,* **10,** 2782–2795.

Siegel, D. A., J. C. Ohlmann, L. Washburn, R. R. Bidigare, C. T. Nosse, E. Fields, and Y. Zhou, 1995: Solar radiation, phytoplankton pigments and the radiant heating of the equatorial Pacific warm pool. *J. Geophys. Res.,* **100,** 4885–4891.

Sprintall, J., and M. Tomzak, 1992: Evidence of the barrier layer in the surface layer of the Tropics. *J. Geophys. Res.,* **97,** 7305–7316.

Sui, C.-H., X. Li, K.-M. Lau, and D. Adamac, 1997: Mutiscale air–sea interactions during TOGA COARE. *Mon. Wea. Rev.,* **125,** 448–462.

Webster, P. J., and R. Lukas, 1992: TOGA COARE: The TOGA coupled ocean–atmosphere response experiment. *Bull. Amer. Meteor. Soc.,* **73,** 1377–1416.

——, C. A. Clayson, and J. A. Curry, 1996: Clouds, radiation, and the diurnal cycle of sea surface temperature in the tropical western Pacific. *J. Climate,* **9,** 1712–1730.

Weller, R. A., and S. P. Anderson, 1996: Surface meteorology and air–sea fluxes in the western equatorial Pacific warm pool during the TOGA Coupled Ocean–Atmosphere Response Experiment. *J. Climate,* **9,** 1959–1990.

Wentz, F. J., 1994: User's Manual SSM/I-2 Geophysical Tapes. Tech. Rep. 070194, 20 pp. [Available from Remote Sensing Systems, Santa Rosa, CA 95404.]

Zhang, C., 1996: Coherence between SST and atmospheric variability in the western Pacific warm pool. Preprints, *Eighth Conf. on Air–Sea Interaction and Conf. on the Global Ocean–Atmosphere–Land System (GOALS),* Atlanta, GA, Amer. Meteor. Soc., J112–J116.

Zhang, Y.-C., W. B. Rossow, and A. A. Lacis, 1995: Calculation of surface and top of atmosphere radiative fluxes from physical quantities based on ISCCP data sets. Part 1: Method and sensitivity to input data uncertainties. *J. Geophys. Res.,* **100,** 1149–1165.